



Analysis of the Kinematic and Radiative Impacts on Sea-ice of a Robust Late-Summer Cyclogenesis Event in the Arctic

Ian C. Beckley¹, Claire Mundi¹, Tristan L'Ecuyer², and Jonathan E. Martin¹



¹Department of Atmospheric & Oceanic Sciences, University of Wisconsin-Madison

²Cooperative Institute for Meteorological Satellite Studies, University of Wisconsin-Madison

On 14 August 2010 a summer cyclone developed at the northern tip of Scandinavia and began an eastward progression across the Barents Sea. Over the next several days it developed rapidly and became stationary just west of Novaya Zemlya on 17 August. Between 00 UTC 15 August and 00 UTC 16 August (Figs. 1a and 1b) the central pressure of the storm deepened 20 hPa to 974 hPa where it remained for the next 24 hour (Fig. 1c).

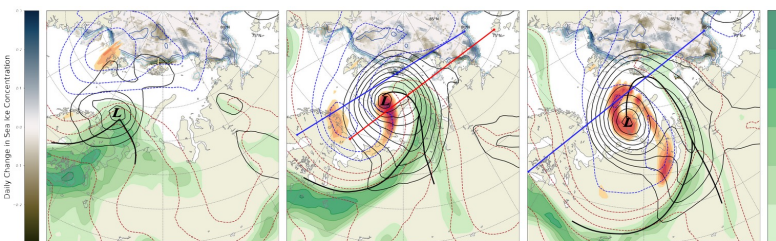


Fig. 1 (a) JRA-55 reanalysis depiction of sea-level pressure (black contours every 4 hPa up to 1012 hPa), 1000-500 hPa thickness (blue/red dashed lines every 60 m), 500 hPa geostrophic relative vorticity (orange shading contoured every $3 \times 10^{-5} \text{ s}^{-1}$ beginning at $12 \times 10^{-5} \text{ s}^{-1}$) and NSIDC sea ice concentration (blue contours every 20%) at 00 UTC 15 August 2010. (b) As for (a) but for 00 UTC 16 August 2010. (c) As for (a) but for 00 UTC 17 August 2010.

Throughout this period the storm became well occluded (see 1000-500 thickness contours in Figs. 1b and 1c) with a cloud shield that dramatically testified to this fact (Figs. 2a and 2b). A vertical cross-section directly through the occluded thermal ridge at 00 UTC 16 August (Fig. 3), illustrates the canonical occluded thermal structure of this robust cyclone. Note that the upper troposphere between the cold and warm frontal portions of the occluded structure was characterized by subtropical-like, low PV air (Fig. 3, shading).

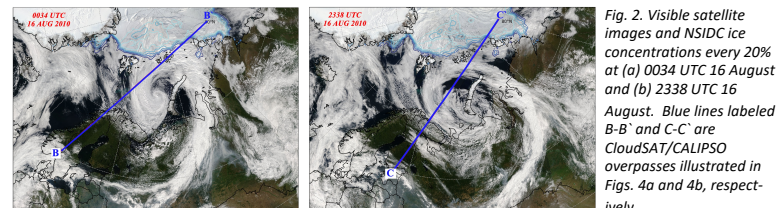


Fig. 2. Visible satellite images and NSIDC ice concentrations every 20% at (a) 0034 UTC 16 August and (b) 2338 UTC 16 August. Blue lines labeled B-B' and C-C' are CloudSAT/CALIPSO overpasses illustrated in Figs. 4a and 4b, respectively.

CloudSAT/CALIPSO overpasses afforded insights into the cloud and precipitation structure of this storm at near 00 UTC on both 16 and 17 August. The 00 UTC 16 August cross-section cuts through the northern periphery of the occluded quadrant and reveals a broad swath of high reflectivity in the heart of the occluded thermal structure (Fig. 4a.) The 00 UTC 17 August lidar retrieval cuts through the occluded cloud head in two places (Figs. 4b and 5) and reveals predominantly mixed phase clouds (Fig. 5a). The western precipitation maxima featured vigorous snowfall and a net-positive cloud

Fig. 3. Vertical cross-section along line A-A' in Fig. 1b of θ (green lines, every 3K), potential vorticity (PV) less than 0.5 PVU (pink) and the 2 PVU dynamic tropopause (black) at 00 UTC 16 August 2010 from JRA-55 data.

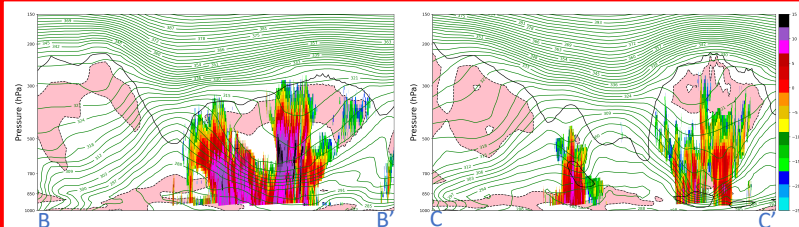


Fig. 4. Vertical cross-sections along B-B' in Fig. 2a (left) and C-C' in Fig. 2b (right) of JRA-55 θ (green lines, every 3K), potential vorticity (PV) less than 0.5 PVU (pink), the 2 PVU dynamic tropopause (black) and corresponding CloudSat/CALIPSO reflectivity granules at 00 UTC 16 and 17 August 2010.

radiative effect (Figs. 5b and 5c). A discrete rainfall maxima was observed within the locally warm, occluded thermal structure associated with the storm's northeastern cloud band (Fig. 4b and 2b). While long-wave radiative heating was remarkably consistent between precipitating regions (Fig. 5c), the moisture-laden environment of the northeastern occluded quadrant appears to have bolstered a highly reflective cloud head and a net negative radiative effect (Figs. 1c and 5b). Substantial ice loss was observed on 00 UTC 17 August at the intersection of the eastern cloud head and the ice edge, likely the result of strong on-ice flow and warm air advection in the lower troposphere (Fig. 1c).

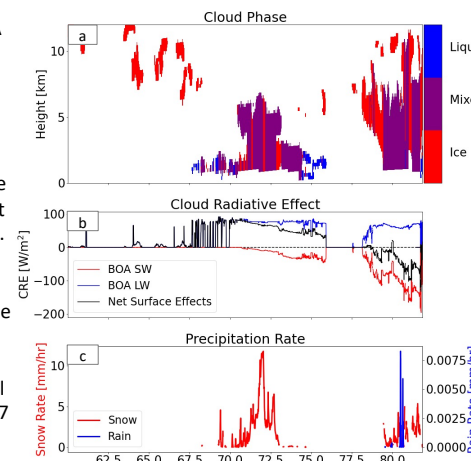


Fig. 5. CloudSat/CALIPSO retrievals of (a) cloud phase, (b) cloud radiative effect and (c) precipitation rate along C-C' at 2338 UTC 16 August 2010.

Conclusions

- Substantial ice losses where the occluded, thermal ridge intersected the MIZ (Fig. 1c) on 17 Aug 2010 were coincident with a net negative radiative effect (Fig. 5b).
- A strong dipole in daily ice change saddles the storm center, with on-ice (off) flow associated with local ice concentration losses (gains) (Figs. 1b and 1c).
- The relative ice area trend became negative upon the cyclone reaching maturity on 16 Aug 2010. The relative trend remained negative through cyclogenesis (Fig. 8b).

Acknowledgments: Funding provided under NSF grant #1951757

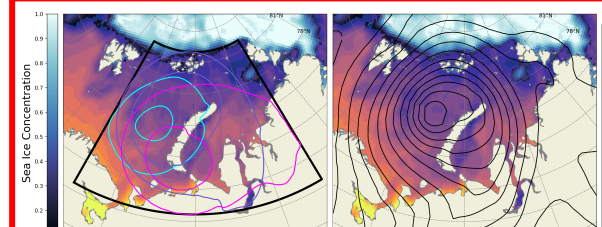


Fig. 6 (a) Ice loss study area (heavy black) with the ERA 990 and 1000 hPa isobars on the 15/16/17 August 2010 (blue/purple/pink). NSIDC sea ice concentration and NOAA optimum interpolation sea surface temperature on 15 Aug 2010 are shaded. (b) As for (a) but with sea-level pressure, sea ice concentration, and SSTs for 00 UTC 16 August 2010.

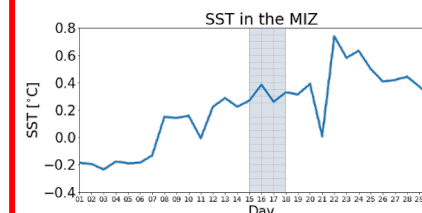
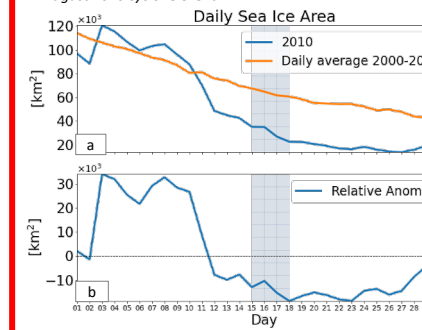


Fig. 7. Daily sea surface temperature within the marginal ice zone, defined as the region with sea ice concentration between 15% and 80%. The grey region highlights the mid-August 2010 cyclone event.



Future Work

- Apply the foregoing analysis techniques to a CloudSat/CALIPSO era catalog of vigorous cyclones which interact with Arctic sea ice in the late summer
- Place this novel analysis method in the context of existing literature concerning high-frequency sea-ice variability
- Incorporate additional CloudSat/CALIPSO variables to gain further insight into the role radiation plays in modulating sea ice on meso/synoptic scales

Another potential ice loss mechanism is the presence of above-freezing sea surface temps (SSTs) in the marginal ice zone (MIZ), defined as the region with ice concentrations between 15% and 80% (Fig. 7). West (east) of the cyclone center off (on)-ice flow potentially advects the MIZ into warmer (cooler) sea surface temperatures (Fig. 6b) with a net warming of SSTs within the MIZ during the cyclone life cycle (Fig. 7, shading). The sea-ice area recedes faster than climatology for two days after the cyclone reaches maturity on 16 Aug 2010 (Figs. 8a and 8b). Over the following week, the trend in ice area remains indistinguishable from climatology.

Fig. 8. (a) Daily sea ice area averages from 2010 as well as a climatological average from 2000-2019 for the study area defined in Fig. 6a. (b) Difference between the 2010 and climatological area anomalies.